2012 IEEE/RSJ International Conference on
Intelligent Robots and Systems
October 7-12, 2012. Vilamoura, Algarve, Portugal

Modeling and Simulation of Friction Forces during Needle Insertion Using Local Constraint Method

Lijuan Wang, Zhongkui Wang and Shinichi Hirai

Abstract— **In modern clinical practices, accurate orientation for needle-like tools inserting into soft tissues is cumbersome, mainly due to the tissue's non-linear deformation and the complicated combination of forces between the tissue and the tool. In this paper, the interaction between tissue deformation and friction forces has been discussed. We consider the relative velocity and contact length as the main factors of friction force during tissue deforming. An available friction model has been built for dynamic needle insertion simulation based on Finite Element (FE) framework. A Local Constraint Method (LCM) is proposed to calculate the tissue deformation and apply the friction forces to the tissue frame for avoiding remeshing. In our approach a series of equivalent constraints and forces are generated by decomposing them inside Local Regions (LRs) to nodal points. Simulations based on this method to realize the dynamic needle insertion have been conducted for validation.**

I. INTRODUCTION

Modern clinical practice in procedures, such as biopsies, prostate brachytherapy, and neurosurgery often involves deep insertion using needle-like tools into soft inhomogeneous tissues [1]. Accurate orientation beneath the tissue surface during these procedures is difficult to achieve due to tissue deformations and unknown interactions between tools and tissues. Modeling and simulations representing such interactions have been developed in recent years, with the aim to understand the forces and geometric changes involved in medical applications such as robot-assisted surgery, and virtual surgical systems for training and planning. Constructing appropriate mechanics-based models to simulate the interactive behaviors of needle and tissues during insertion has been found challenging.

Over the past two decades, experimental and analytical models that characterize tissue properties, needle forces, needle deflection, and the mechanics of events during needle insertion, such as contact, rupture and friction, have been studied. Modeling for soft objects is the basic for needle insertion. Tissue property has been systematically studied by Fung in his book [2]. The pioneering work of the Needle-Tissue interaction simulation has been done by Dimaio $et\ al.$ They use the low-rank matrix updates to achieve the interactive simulation based on Finite Element Method (FEM) [3], [4]. Simone and Okamura developed an empirical force model for soft tissue penetration. Needle forces were considered as a combination of stiffness force, friction and cutting forces [5], [6]. Mahvash and Dupont contributed to knowledge of the mechanics of rupture events with a dynamic model [7]. They showed that a higher velocity of needle insertion reduces the force of a rupture event. A review work in this field has been presented by Abolhassani, 2007 [1], and Misra, 2008 [8].

Many needle insertion experiments show that the friction force plays an important role among the complicated sources of needle forces. In the work of Okamura [6], they described the friction model using a modified Karnopp model due to tissue adhesion and damping. Kobayashi $et\ al.$ proposed the friction force based on the relative velocity between the needle and liver tissue ranging from hyper slow velocity and verified their model through experiments [9]. However, their models are mainly focus on the relationship between friction force and relative velocity, with less consideration of the influences by tissue deformation during the dynamic insertion procedures.

In this paper, the interaction between tissue deformation and friction forces has been discussed during the dynamic insertion procedure. We consider the relative velocity and contact length as the main factors of friction forces with tissue deforming. A friction model has been built for dynamic needle insertion simulation based on a rigid needle and a viscoelastic tissue. Remeshing is normally required due to the conflict between continuous movement of the needle and discontinuous FE frameworks. In our approach, we proposed a Local Constraint Method (LCM) to generate a series of equivalent constraints and forces by decomposing them inside Local Regions (LRs) and applying them to nodal points. Simulations based on this method to realize the dynamic needle insertion have been conducted for validation.

The paper is organized as follows. In Section II we have a brief review of the relative work in needle insertion modeling and simulation. We analyze the friction force based on tissue deformation during insertion in Section III. In Section IV, the dynamic model has been presented and our approach for applying the friction force during needle insertion using the LCM has been detailed. Simulations and experiments are given in Section V. Conclusions and future work appear in the final section.

II. PREVIOUS WORK

Models and simulations for needle insertion into soft tissues have been investigated by many researchers. The motivation of our research is to generate an available physical-based dynamic model for needle-tissue interaction considering both information of interactive forces and tissue

This work was supported in part by Grant in Aid for Scientific Research (No.2324604) and R-GIRO Program of Ritsmeikan University.

The authors are with Department of Robotics, Ritsumeikan University, Noji-higashi 1-1-1, Kusatsu, Shiga, Japan gr0081vf@ed.ritsumei.ac.jp, wangzk@fc.ritsumei.ac.jp, and hirai@se.ritsumei.ac.jp

deformation. As we have mentioned, relative researches in this field include the physical-based models for soft tissue with different properties [2], models for steerable needle [10], [11], and the analysis for events happened during insertion procedure such as rupture mechanism [7] as well as different sources of forces such as friction [9].

In the work of Okamura [6], they present the needle force during needle insertion is a summation of stiffness, cutting, and friction forces and they separate the insertion course into pre-puncture and post-puncture phases. However, for different materials, the main factor of needle force is different. For example, in some moisture-rich organs, the friction force is very small and the needle force during insertion tends to be constant, which can be considered as only the cutting force. In some other tissues with less lubrication, friction force may become the major part of the total force. In this paper, we focus on the frictional phenomenon, based on one kind of artificial human muscle in which the friction plays the main role in the total needle force.

There are several friction models for soft objects, such as Karnopp friction model [12], models considering the Stribeck effect [13], and the Dahl model [14], which includes pre-sliding displacement. For needle insertion, in [6], they employ a modified Karnopp friction model to analysis the friction based on experimental data. In the work of [9], they build an empirical model with parameter identification for friction force.

To improve the simulation accuracy, we employ the Finite Element Method for our dynamic model. Dynamic modeling and parameter identification based on FEM for soft, deformable materials have been studied in our previous work [15], [16]. In this paper, parameters such as the local relative velocities and the contact lengths can be obtained due to the mechanism of tissue deformation. The distribution of needle forces and displacement constraints have been applied to affect the deformation as well. Also, a Local Constraint Method has been improved to deal with the approximation of transforming the needle friction effect inside tissue elements to its nodes on the frame.

Figure 1 shows an example to interpret the main idea of our approach. When the needle contact with the tissue before puncture, there is no friction force due to the contact length along the needle shaft is zero, as shown in Fig. 1a. After puncture, the needle's tip is inside one triangle element of the tissue (the yellow one) as $E_{P_1P_5P_4}$ in Fig. 1b. With considering tissue deformation, we can obtain the contact length of $N_{Tip}P_4$ and the average relative velocity v_1^* between the needle and the element $E_{P_1P_5P_4}$. Friction force can be calculated by length of $N_{Tip}P_4$ and v_1^*. Then we decompose the friction force to nodal points P_1, P_5, and P_4 (red points) in $E_{P_1P_5P_4}$ to solve the equation of motion for tissue deformation. When the needle is inserted into the second triangle $E_{P_1P_2P_5}$, we consider the friction forces in two contacted elements. Similarly, we can respectively calculate the forces using contact lengths and the relative velocities inside $E_{P_1P_5P_4}$ and $E_{P_1P_2P_5}$. Here, we propose an

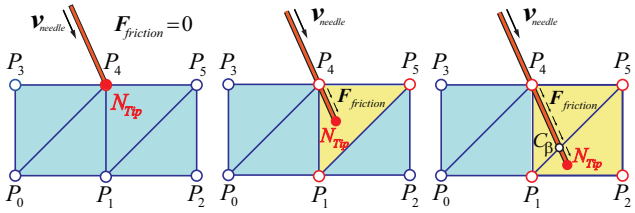

(a) Pre-puncture (b) Insert one element (c) Insert two elements

Fig. 1: An example of LCM for friction modeling.

linear approximation to get the intersecting point C_β. Thus a simulation of friction during insertion considered tissue deformation without remeshing is realized. More details are given in following sections.

III. Friction Modeling during Needle Insertion

In needle insertion, there is complicated interdependent relationship between the tissue deformation and the friction force. On one hand, friction forces occur along the contacted needle shaft, which mainly affect the tissue deformation as external forces. On the other hand, the nonlinear tissue deformation leads to a nonlinear distribution of relative velocities between the needle and the contacted tissue elements. The varied relative velocity and the time dependent tissue deformation also influence the values and the distribution of friction forces.

According to previous work on the friction model for needle insertion and soft objects[6], [9], in generally, friction force is related to tissue properties, and the relative motion between the two contact objects. In the experiments, they sandwiched the tissue by plastic plates in order to avoid the influence of tissue deformation. Finally they obtained the function of friction force respect to relative velocity and some tissue parameters. However, their models take less consideration of tissue deformation, and the measured friction forces are under certain tissue thickness.

Here, we consider two factors to express the frictional phenomenon. One is the relative velocity $\mathbf{v}^*$ between the tissue and the needle, which varies along the needle shaft depending on each contact point. The other is the contact length l_c, which is defined as the tissue-contacted length along the needle shaft and respected to the needle motion and tissue deformation. We assumed that the tissue is homogenous and parameters for tissue properties are unchanged while its deforming.

Under the assumptions above, we firstly defined the distribution coefficient of friction force $\mathbf{R}_f$ as follows:

$$\mathbf{R}_f(\mathbf{v}^*) = \frac{\mathbf{F_{friction}}}{2\pi r L_c}, \tag{1}$$

where r and L_c respectively denote the radius of needle and the test tissue thickness, and $\mathbf{F_{friction}}$ is the friction force with respected to relative velocity under the constant tissue thickness L_c. Note that, the distribution coefficient $\mathbf{R}_f$ is fixed for a given relative velocity $\mathbf{v}^*$.

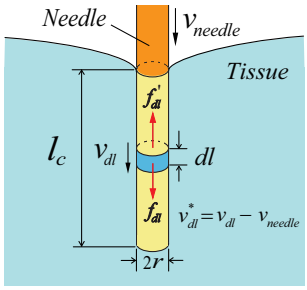

Fig. 2: The scheme of the friction model during needle insertion process.

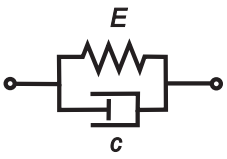

Fig. 3: Kelvin-Voigt Model used to describe the viscoelastic force-deformation behavior in virtual tissue.

Then, we consider the total friction force during the dynamic insertion procedure. The scheme of the friction model is shown in Fig. 2. We separate the contact tissue surface into small regions along the needle shaft with length dl. So the contact areas of this region can be calculated as $2\pi r dl$. As a result, the total friction force is considered as an integral of friction forces applied on the needle as follows:

$$\mathbf{F_{friction}} = \int_0^{l_c(t)} 2\pi r \mathbf{R}_f(\mathbf{v}^*) dl. \tag{2}$$

IV. Dynamic Modeling based on Local Constraint Method

Modeling the needle-tissue interaction using the FEM is challenging because the invasive process involves multiple remeshing which is computationally expensive for simulation [8]. In this section, we propose the dynamic model for needle insertion with a viscoelastic behavior tissue based on FEM in 2D, introduce the main algorithm of the Local Constraint Method (LCM), and detail its application for friction force. In this work, we focus on the friction force. So we assume the needle to be rigid and with sharp tip to ignore the needle deformation and the rupture mechanism.

A. Dynamic Model for Needle Insertion

In our model, the deformable tissue is represented by a Kelvin-Voigt model as shown in Fig. 3. Tissue property is assumed to be uniform and isotropic. We use four Lamé's constants, λ^{ela}, μ^{ela} , λ^{vis}, and μ^{vis} to characterize both the elasticity and viscosity properties respectively for each triangle element in the FE frame. They are defined as follows,

$$\lambda^{ela} = \frac{E\upsilon}{(1+\upsilon)(1-2\upsilon)}, \mu^{ela} = \frac{E}{2(1+\upsilon)},$$
$$\lambda^{vis} = \frac{\upsilon^{vis} c}{(1+\upsilon^{vis})(1-2\upsilon^{vis})}, \mu^{vis} = \frac{c}{2(1+\upsilon^{vis})}, \tag{3}$$

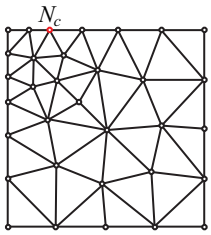

Fig. 4: Body frame initialization with the surface-contact point N_c.

where E and c denote the elastic and viscous moduli respectively; and Poisson ratios are given by υ and υ^{vis}.

The body frame is generated at the moment when the needle tip is considered to be contact with the tissue surface. We consider the surface contact point on tissue N_C as a nodal point of the frame, using a free software 'Mesh 2D' by Engwirda [18] to generate the triangular meshes automatically. An example of generated body frame after surface contact is shown in Fig. 4. As a result, we can express the surface deformation including the arbitrary contact point.

After mesh generation, connection matrices of the body frame are created as J_λ and J_μ, which can be obtained by synthesizing partial matrices together to describe the geometric relationship within the structure. Let the vector $\mathbf{u}_N$ denote the displacement of all nodal points, and $\dot{\mathbf{u}}_N$ denotes the velocity, the internal viscoelastic forces can be formulated as:

$$\mathbf{F}_{visela} = \left(\lambda^{ela} J_\lambda + \mu^{ela} J_\mu\right) \mathbf{u}_N + \left(\lambda^{vis} J_\lambda + \mu^{vis} J_\mu\right) \dot{\mathbf{u}}_N. \tag{4}$$

During the insertion simulation, we suppose the bottom of the tissue is fixed. The bottom constraint R_{bt} is described as

$$R_{bt} : A_{bt}\mathbf{u}_N = 0,$$

where A_{bt} denotes the constraint matrix which selected the bottom nodes to be full-constrained. To incorporate the constraint into the numerical computation of differential equations, we apply the constraint stabilization method (CSM)[17]. Then we have the bottom constraint equation as:

$$A_{bt}^T \ddot{\mathbf{u}}_N + 2\omega A_{bt}^T \dot{\mathbf{u}}_N + \omega^2 A_{bt}^T \mathbf{u}_N = 0, \tag{5}$$

where ω is a predetermined angular frequency.

In the whole needle insertion process, the condition of constraints varies in different periods. The situation with different interactions between needle and the contacted tissue part need to be discussed. However the influence of these interactions to the dynamic model can be considered in two aspects, the external forces and displacement constraints. As a result, the equations of motion can be written as follows:

$$\begin{cases} M\ddot{\mathbf{u}}_N = -\mathbf{F}_{visela} + \mathbf{F}_{ext} + \lambda A_{con} \\ R_{con} : A_{con}^T (\mathbf{u}_N - \delta) = 0 \end{cases} \tag{6}$$

where λ is the Lagrange multiplier and M denotes the inertia matrix of the tissue. The constraint equation R_{con} is defined as a combination of displacement constraints of the nodal points, including bottom constraint. Matrix A_{con}

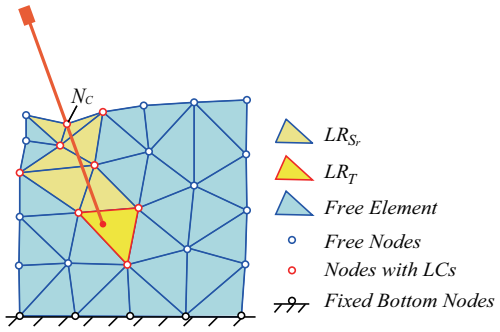

Fig. 5: A series of Local Regions along the needle.

denotes the total displacement constraint matrix, which select the nodes to be fully or partially constrained, and δ is a vector of constraint distance. The total vector of the extra force is expressed by $\mathbf{F_{ext}}$, including the effects of external forces acting on nodal points, such as cutting force and friction. Note that $\mathbf{F_{ext}}$, A_{con}, and R_{con} are respected to time according to different periods during insertion.

B. Local Constraint Method

We consider the effects on tissue by needle movements in two aspects: the external force $\mathbf{F}_{ext}$ and displacement constraints R_{con}, as in (6). External forces are applied to tissue by the needle, based on physical phenomena. Displacement constraints are respected to the geometrical boundaries of the two objects while they contact with each other.

For insertion, after needle tip punctures the tissue's surface, the needle is considered to be inside the tissue. The constraint between the two objects should be continuous. However, in the FEM, tissue's behaviors are approximated by a series of elements connected by discrete nodes. The conflict between discrete frame and continuous constraints is to be tackled. Frequent remeshing which has been widely used for needle insertion simulation is computationally expensive.

To avoid remeshing while achieve precise approximate results, the LCM is to transfer the constraint inside elements to nodes as Local Constraints (LCs). The global constraint will be a combination of all LCs' contributions. We define a series of elements connected with both the needle's tip and shaft as the Local Region (LR), as shown in Fig. 5. According to the different part the region connected, we divide LRs into two types:

- LR_T is defined as the element contact with the needle tip in current time. It will be replaced when the needle tip contact with a different element.
- LR_{S_r} $(r = 1, 2, ..., N-1)$ is defined as the element which is connected with the needle along the shaft, excluding LR_T. Note that, the subscript r denote the order of tip contact during insertion, and N shows the total number of all contact regions in current time.

The global constraint is considered as a combination of all constraints including the constraint on nodes, such as at the contact node N_C and the bottom nodes N_B, as well as the constraint applied on each LR. The steps of the constraint method in our dynamic model are as follows. Firstly we do the contact detection to find LRs in current time. For each LR, according to its constraint type, equivalent constraints or applied external forces for each nodal point are calculated, using the information of the needle and the region's nodes, such as positions and velocities. After that, the equation of motion with the global R_{con} and $\mathbf{F}_{ext}$ is updated. Solve the equation, finally we have the tissue deformation and the forces.

C. Realization of Friction Force

In Section II we have mentioned that the total friction force can be described as an integral of forces along the needle shaft with the consideration of both the contact length and relative velocities, in (2). To apply the distribution of friction forces to the dynamic needle insertion model, we employ the LCM for the simulation. A realization of friction forces during insertion process is detailed in this section, under a constant preset needle velocity $\mathbf{v}_{needle}$.

1) Contact Detection for Local Regions: In contact detection, a 'distance' Δ_{tip} has been used to 'measure' the relative position between the needle tip and each element of the tissue, which is defined as

$$\Delta_{tip} = \begin{vmatrix} \xi_{tip} & \xi_j \\ \eta_{tip} & \eta_j \end{vmatrix} + \begin{vmatrix} \xi_j & \xi_m \\ \eta_j & \eta_m \end{vmatrix} + \begin{vmatrix} \xi_m & \xi_{tip} \\ \eta_m & \eta_{tip} \end{vmatrix}. \quad (7)$$

We define current coordinates of nodal points in the triangle element $\Delta P_i P_j P_m$ as (ξ_c, η_c), where $c = i, j, m$, denote the name of these points in a counterclockwise order as P_i, P_j and P_m. The current coordinates of the needle tip are as (ξ_{tip}, η_{tip}). The value of Δ_{tip} will be positive, negative, or zero respectively when the needle tip is inside, outside, or on the edge of the triangle. As a result, we can find out the relative position between the needle tip and tissue elements, the latest tip-contacted region is considered as the LR_T.

As the needle first contacts the tissue surface, the initial frame of tissue body is generated, as shown in Fig. 3. After puncture, a series of LRs are detected in order and recorded in LR_array. For example, as LRs distributed along the needle in Fig. 5, we have

$$LR\_array = No.tri\left(LR_{S_1}, LR_{S_2}, \cdots, LR_{S_{N-1}}, LR_T\right). \quad (8)$$

We update LR_array when the needle tip is inside a new LR or divorce from the old LR_T in a reverse movement.

2) A Modified Friction Model Based on LRs: In the consideration of the friction model under an FE frame, we separate the contact length during insertion according to LRs. The total friction force $F_{friction}$ has been modified as the sum of forces acting on LRs,

$$\mathbf{F_{friction}} = \sum_{k=1}^{N} \left(2\pi r \mathbf{R_f}\left(\mathbf{v_k^*}\right) l_k\right), \quad (9)$$

where the contact length and the relative velocity in LR_k are defined as l_k and $\mathbf{v}_k^*$ respectively. Note that in the reality $\mathbf{v}_k^*$ is not a constant even inside a contacted tissue element. We approximate velocity $\mathbf{v}_k^*$ by the average relative velocity

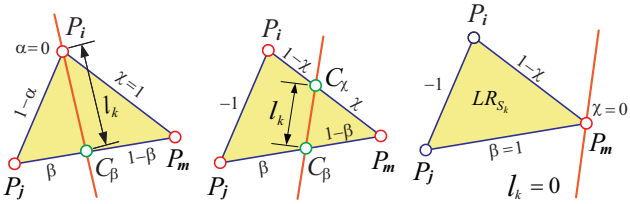

(a) Node-edge (b) Double-edge (c) Single-node

Fig. 6: The contact length of LR_{S_k} in different contact types.

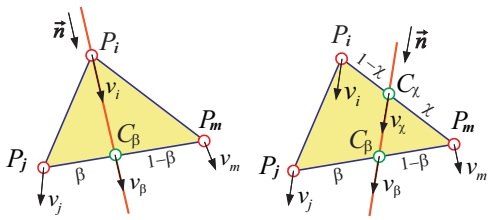

(a) Node-edge (b) Double-edge

Fig. 7: Velocities in LR_{S_k} of two typical contact types.

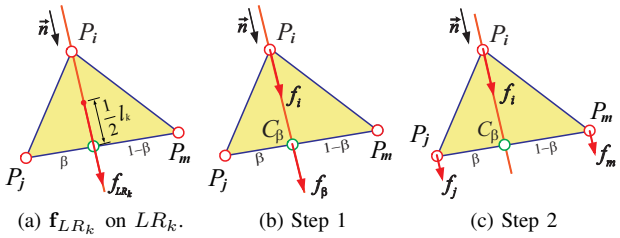

(a) $\mathbf{f}_{LR_k}$ on LR_k. (b) Step 1 (c) Step 2

Fig. 8: A proximate division for applying the friction force onto frame inside LR_{S_k}.

along the contact length of the LR_k. To obtain the local contact length l_k, we need to consider the contact situation of each LR_k.

3) Contact Length in LRs: For a shaft-contact region LR_S, there are three typical contact types between the needle shaft and the region, as shown in Fig. 6. We define a *ratio vector* $\mathbf{P_k}$ to describe the relative position between the needle and LR_{S_k}:

$$\mathbf{P_k} = \begin{bmatrix} \alpha & \beta & \chi \end{bmatrix}^T. \tag{10}$$

We define α, β, and χ as the ratios on the edges of P_iP_j, P_jP_m, and P_mP_i respectively, where α, β, and χ are in the range of $[0, 1]$. Specially, if there is no contact point on the edge, we set the ratio value to -1.

Note that the distance between nodal point and the needle shaft may change due to tissue deformation. However, the ratio factors of the relative position varies in small ranges. We assume the ratios for each LR_{S_k} is unchanged after the region is shaft-contacted. Then the contact length can be described with the coordinates of nodal points and the ratios according to the contact situation. For example, let $\mathbf{C}_\beta$ and $\mathbf{C}_\chi$ be coordinates of P_β and P_χ in Fig. 6b; $\mathbf{P}_c$ denotes coordinates of the nodal points, where $c = i, j, m$. Then the contact length l_k of LR_{S_k} is

$$l_k = |\mathbf{C}_\beta - \mathbf{C}_\chi|, \tag{11}$$

where

$$\mathbf{C}_\beta = (1-\beta)\,\mathbf{P}_j + \beta\mathbf{P}_m,$$
$$\mathbf{C}_\chi = (1-\chi)\,\mathbf{P}_m + \chi\mathbf{P}_i.$$

4) Relative Velocity of LRs: As we have mentioned in the modified model in (9), $\mathbf{v}_k^*$ is defined as the average relative velocity which contributes the friction force of LR_k through the length dl_k. To obtain $\mathbf{v}_k^*$, we consider the first two contact types: Node-edge and Double-edge contact, for the *contact length* is non-zero.

In the Node-edge contact, as shown in Fig. 7a, the needle is contacted through the length between a nodal point P_i and a edge point C_β. We denote $\mathbf{n}$ as the direction vector of the needle axis. The current velocities at nodal points P_i, P_j, P_m are $\mathbf{v}_i$, $\mathbf{v}_j$, and $\mathbf{v}_m$ respectively. As they contact through the needle shaft, the movement of the shaft-contact point as P_i and C_β are restricted, and the velocities at those points are all along the direction of needle axis. According to the linear approximation in FEM, we propose the average velocity along the contact length as

$$\overline{\mathbf{v}}_k = \frac{1}{2}\left(\mathbf{v}_i + \mathbf{v}_\beta\right), \tag{12}$$

where

$$\mathbf{v}_\beta = \mathbf{n}^T \cdot \left[(1-\beta)\mathbf{v}_j + \beta\mathbf{v}_m\right].$$

Then we can calculate the relative velocity of LR_k using the average velocity of the contact length. As we consider the needle velocity as $\mathbf{v}_{needle}$, let us project it onto the direction of needle axis. Finally we have the relative velocity of LR_s as

$$\overline{\mathbf{v}}_k^* = \overline{\mathbf{v}}_k - \mathbf{n}^T \cdot \mathbf{v}_{needle}. \tag{13}$$

Similarly, in the $Double-edge$ case as in Fig. 7b, the relative velocity $\mathbf{v}_\mathbf{k}^*$ can also be calculated in (13). The average velocity is calculated as

$$\overline{\mathbf{v}}_k = \frac{1}{2}\left(\mathbf{v}_\beta + \mathbf{v}_\chi\right), \tag{14}$$

where the velocities on C_β and C_χ are

$$\mathbf{v}_\beta = \mathbf{n}^T \cdot \left[(1-\beta)\mathbf{v}_j + \beta\mathbf{v}_m\right],$$
$$\mathbf{v}_\chi = \mathbf{n}^T \cdot \left[(1-\chi)\mathbf{v}_m + \beta\mathbf{v}_i\right].$$

5) Realization of Friction Forces on the FE Frame: Based on the contact length and the average relative velocity in a local region, we can approximate the local friction force $\mathbf{f}_{LR_k}$ as a sum of distributed friction forces in LR_k. Force $\mathbf{f}_{LR_k}$ can be written as

$$\mathbf{f}_{LR_k} = 2\pi r \mathbf{R}_f(\mathbf{v}_k^*) \cdot l_k. \tag{15}$$

For instance, we consider the realization of friction in the Node-edge contact case on a single tissue element LR_k.

As a product of the average relative velocity, we apply the local friction force $\mathbf{f}_{LR_k}$ on the center of the contact length,

as shown in Fig. 8a. Our objective is to transfer the local friction force back to the tissue frame. We separate the force simply in two steps. Firstly, the local force is distributed to the end points of the contact length, P_i and C_β as shown in Fig. 8b. We generally have

$$\mathbf{f}_i = \mathbf{f}_\beta = 2\pi r \mathbf{R}_f(\mathbf{v}_k^*) \cdot \left(\frac{1}{2} l_k\right). \tag{16}$$

In step 2, we separate the force on edge point C_β to its edge nodes P_j and P_m, with the consideration of the ratio β. Let $\mathbf{f}_j$ and $\mathbf{f}_m$ denote the forces on P_j and P_m, as in Fig. 8c. We have

$$\mathbf{f}_j = (1-\beta)\,\mathbf{f}_\beta, \text{and } \mathbf{f}_m = \beta \mathbf{f}_\beta. \tag{17}$$

As a result, for each LR, we have the forces on its nodal points to approximate the influence of friction. Combining all the nodal friction force of LRs, we can finally have the friction force as the contribution of $\mathbf{F}_{ext}$ for the dynamic model.

V. Simulations and Experiments

To validate the friction model and the local constraint method, simulations and experiments have been conducted in this section.

A. Simulations

We simulate a two dimensional dynamic model of insertion with a viscoelastic tissue. The tissue is a rectangle of $80 \times 80\,\text{mm}^2$. Elastic and viscous moduli are $E = 20\,\text{kPa}$ and $c = 20\,\text{kPa}$. Poisson ratios are given by $\nu = \nu^{vis} = 0.35$. The needle is assumed as a rigid one and its motion during the insertion is preset. During the first 2 s, the needle moves along the direction of its axis at a velocity of 13 mm/s, and then be static for 2 s inside the tissue. After that the needle moves inversely at 13 mm/s for 2 s and finally stay still. The angle θ_{Pos} is defined to describe the posture of the needle.

Figure 9 shows simulation snapshots of insertion procedure. The initial state of this simulation is shown in Fig. 9a When the needle's tip first reaches the top of the tissue, the tissue frame is generated as in Fig. 9b. Then the needle is inserted into the tissue. Tissue deforms due to the friction force applied by the needle Fig. 9c. When the needle stops inside, the tissue partly recovers as in Fig. 9d. After that, as the needle retreats in Fig. 9e, the tissue is dragged by needle at first; and after separate from the needle, the tissue releases as in Fig. 9f.

Figure 10 shows the friction force performance in this simulation. In this simulation, to focus on friction modeling, we assume the needle is sharp and rigid, so that we do not consider the rupture, cutting force, as well as the needle's deformation. In Fig. 10a, we measure the distance between the needle's tip and its first contacted point on surface, as the *contact length* l_c. Figure 10b shows an example of a nodal point's relative velocity varies according to the needle-tissue interactions. Figure 10c is the total bottom force which can be compared with the experimental results of the needle force, however when the needle is removed from the tissue, the needle force will reduce to be zero, while the bottom force varies slower due to tissue deformation and the inertia force.

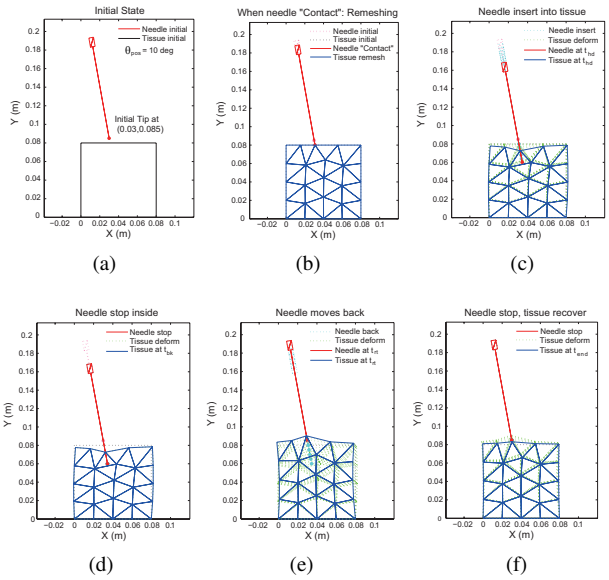

Fig. 9: Simulation snapshots of a rigid needle inserting viscoelastic tissue in 2D.

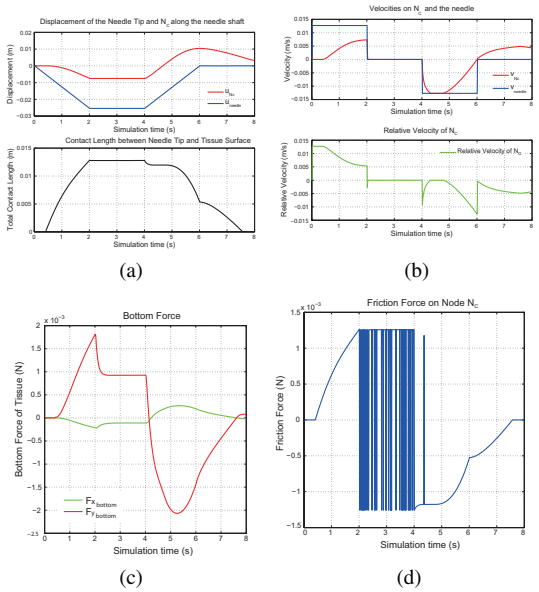

Fig. 10: Simulation results. (a) contact length, (b) relative velocity, (c) bottom force, (d) friction force on N_c.

As we discussed in our friction force model, we consider two main factors of the friction force during the needle insertion procedure, the contact length and relative velocity. Through the simulation results, we find out the main contributions of the two factors. In this simulation we use the simplest friction force function as,

$$f_{friction} = \begin{cases} Kl_c & v^* > 0 \\ -Kl_c & v^* < 0 \end{cases}. \tag{18}$$

As shown in Fig. 10d, the result shows that when the relative

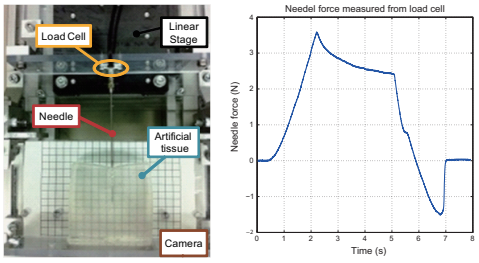

(a) Experiment setup (b) Measured needle force

Fig. 11: Experiment setup and result.

velocity is close to the 'hyper-low' range, the friction varies dramatically. It results the tissue point 'stick' onto the needle at that moment; and when v^* leaves that range, the contact length l_c will dominate the value of the friction force.

B. Experiments

The experiment setup is shown in Fig. 11a. The needle is driven by the Linear Stage, (KX1250C, Suruga Seiki, Japan). One-axis force sensor, (WGI-400A, Tec Gihan Co., Japan) is used to measure the needle force in its insertion direction. A type of artificial 'human muscle' is selected as the insertion object. From some preliminary tests, we find that the friction coefficient of this material is high. We can consider that the friction force plays the main role of the total needle force through the 'muscle'. The result of the needle force measurement during an insert-retreat process is shown in Fig. 11b. By comparing with the simulation results, the trends of the force are almost consistent. However, the identification of the material parameters and friction coefficients will be investigate in the near future.

VI. Conclusion and Future Work

In this paper, we model the friction force acting on needle insertion with considering the tissue deformation. The relative velocity and contact length are the most important factors in our friction model. LCM was employed to calculate the tissue deformation and apply the friction force to the tissue frame. Remeshing was avoided in our simulation of the dynamic needle insertion based on FEM. Simulation results showed the validity of our approach. However, for a complete dynamic needle insertion simulation, modeling of other sources of force is needed. In future, there are two main issues: one is the experiment to evaluate the LCM; the other is to complete the dynamic needle insertion modeling and simulation with considered the stiffness, cutting and friction forces.

References

[1] N. Abolhassani, R. Patel, "Needle insertion into soft tissue: a survey," Medical Engineering and Physics, vol. 29, no. 4, May 2007, pp. 413-431.

[2] Y. C. Fung, Biomechanics: Mechanical Properties of Living Tissues, Springer-Verlag, 1993.

[3] S. P. DiMaio, and S. E. Salcudean, "Needle insertion modeling and simulation," IEEE Trans. Robotics and Automation, vol. 19, no. 5, 2003, pp. 864-875.

[4] S. P. DiMaio, and S. E. Salcudean, "Interactive simulation of needle insertion models," IEEE Trans. Biomedical Engineering, vol. 52, no. 7, 2005, pp. 1167-1179.

[5] H. Kataoka, T. Washio, *et al.*, "Measurement of the tip and friction force acting on a needle during penetration," in Proc. of the 5th International Conference on Medical Image Computing and Computer-Assisted Intervention-Part I, Springer-Verlag, 2002, pp. 216-223.

[6] A. M. Okamura, C. Simone, *et al.*, "Force modeling for needle insertion into soft tissue," IEEE Trans. Biomedical Engineering, vol. 51, no. 10, 2004, pp. 1707-1716.

[7] M. Mahvash, and P. E. Dupont, "Mechanics of dynamic needle insertion into a biological material," IEEE Trans. Biomedical Engineering, vol.57, no.4, Apr. 2010, pp. 934-943.

[8] S. Misra, K. T. Ramesh, and A. M. Okamura, "Modeling of tool-tissue interactions for computer-based surgical simulation: a literature review," Presence: Teleoperators and Virtual Environments, Oct. 2008, vol. 17, no. 5, pp. 463-491.

[9] Y. Kobayashi, T. Sato, and M. G. Fujie, "Modeling of friction force based on relative velocity between liver tissue and needle for needle insertion simulation," In: Engineering in Medicine and Biology Society, 2009. Annual International Conference of the IEEE, 3-6 Sept. 2009, pp. 5274-5278.

[10] R. J. Webster, J. S. Kim, *et al.*, "Nonholonomic modeling of needle steering," The International Journal of Robotics Research, May 2006, vol. 25 no. 5-6, pp. 509-525.

[11] S. Misra, K. B. Reed, *et al.*, "Mechanics of flexible needles robotically steered through soft tissue," The International Journal of Robotics Research, November 2010, vol. 29, no. 13, pp. 1640-1660.

[12] D. Karnopp, "Computer simulation of stick-slip friction in dynamical systems," J. Dynamic Syst., Meas, Contr., vol. 107, Mar. 1985, pp. 100C103.

[13] V. J. Majd and M. S. Simaan, "Continuous friction model for servo systems with stiction," in Proc. IEEE Conf. Control Applications, 1995, pp. 296C301.

[14] P. R. Dahl, "Solid friction damping of mechanical vibrations," AIAA J., vol. 14, Dec. 1976, pp. 1675C1682.

[15] S. Hirai, S. Tomokuni, "Dynamic Modeling of Rheological Deformation," in Proc. of the 2004 JSME Conference on Robotics and Mechatronics Division, Nagoya, 2004, pp. 2A1-H-7.

[16] Z. Wang, K. Namima, S. Hirai, "Physical parameter identification of rheological object based on measurement of deformation and force," in Proc. IEEE International Conf. on Robotics and Automation, 2009, pp. 1238-1243.

[17] S. T. Lin and J. N. Huang, "Stabilization of Baumgarte's using the Runge-Kutta approach", IEEE Conference on Intelligent Robots and Systems, Oct. 1998.

[18] Matlab Mesh2d by Darren Engwirda, 2005-07, available to download at http://www.mathworks.com/ matlabcentral/fileexchange

[19] M. Marchal, E. Promayon, and J. Troccaz, "Simulating prostate surgical procedures with a discrete soft tissue model," 3rd Workshop in Virtual Reality Interactions and Physical Simulation "VRIPHYS", 2006, pp. 109-118.

[20] C. Duriez, C. Gubert, *et al.*, "Interactive Simulation of Flexible Needle Insertions Based on Constraint Models," Medical Image Computing and Computer-Assisted Intervention, Lecture Notes in Computer Science, vol. 5762, 2009, pp. 291-299.

[21] L. Wang, and S. Hirai, "A Local Constraint Method for Needle Insertion Modeling and Simulation," in Proc. of the 10th IEEE International Symposium on Haptic Audio-Visual Environments and Games, Qinhuangdao, China, 2011, pp. 39-44.

[22] R. Alterovitz, K. Goldberg, *et al.*, "Needle insertion and radioactive seed implantation in human tissues: simulation and sensitivity analysis," in Proc. IEEE International Conf. on Robotics and Automation, Taipei, Taiwan, vol. 2, 2003, pp. 1793-1799.

[23] H. W. Nienhuys, and A. F. van der Stappen, "A computational technique for interactive needle insertions in 3D nonlinear material," in Proc. IEEE International Conf. on Robotics and Automation, vol. 2, 2004, pp. 2061-2067